

Exploring stellar evolution with gravitational-wave observations

Irina Dvorkin¹*, Jean-Philippe Uzan¹, Elisabeth Vangioni¹, Joseph Silk^{1,2,3,4}

¹ Institut d’Astrophysique de Paris, Sorbonne Universités, UPMC Univ Paris 6 & CNRS, UMR 7095, 98 bis bd Arago, F-75014 Paris, France

² AIM-Paris-Saclay, CEA/DSM/IRFU, CNRS, Univ Paris 7, F-91191, Gif-sur-Yvette, France

³ Department of Physics and Astronomy, The Johns Hopkins University, Baltimore, MD 21218, USA

⁴ BIPAC, University of Oxford, 1 Keble Road, Oxford OX1 3RH, UK

11 January 2019

ABSTRACT

Recent detections of gravitational waves from merging binary black holes opened new possibilities to study the evolution of massive stars and black hole formation. In particular, stellar evolution models may be constrained on the basis of the differences in the predicted distribution of black hole masses and redshifts. In this work we propose a framework that combines galaxy and stellar evolution models and use it to predict the detection rates of merging binary black holes by Advanced LIGO. A qualitative comparison of several stellar evolution models shows that they differ by the total number of detectable events, and in some cases exhibit model-specific features in the mass distribution, such as peaks and cutoffs. These features, together with the mass-redshift distribution, can be used to discriminate between various stellar evolution models when the number of detected mergers increases.

Key words: binaries, black holes, gravitational waves, galaxies: evolution

1 INTRODUCTION

The discovery of the first gravitational-wave (GW) source GW150914, a merger of two black holes (BHs), by Advanced LIGO (Abbott et al. 2016d) marked the birth of a new astronomical discipline. During the first two Advanced LIGO observing runs two additional sources, as well as a tentative, lower-significance, signal were detected (GW151226, LVT151012, GW170104; Abbott et al. 2016a, 2017). These observations have notably shown for the first time that heavy ($\gtrsim 20M_{\odot}$) BHs exist and can form binaries that merge within the age of the Universe. As the sensitivity of ground-based interferometers increases, future GW observations of merging BH binaries will provide more precise information on their masses, spins and redshifts. Indeed, it is expected that a few tens to a few hundreds of events will be observed within the next several years (Abbott et al. 2016a). This wealth of data can of course be used to study the models that describe how BHs form.

The leading scenario that has been proposed to explain the formation of stellar-mass ($\lesssim 100M_{\odot}$) BHs relies on the standard evolution channel of massive ($\gtrsim 20M_{\odot}$) field stars. After the iron core collapses, a BH can form ei-

ther after a supernova explosion and the following (partial) fallback or matter and eventual collapse, or a direct collapse of the entire stellar envelope (Woosley & Weaver 1995; Belczynski et al. 2010; Fryer et al. 2012; Limongi 2017). An interesting phenomenon occurs in the mass range of $\sim 130 - 250M_{\odot}$ (but note the dependence on metallicity and rotation velocity) where the star becomes unstable due to production of electron-positron pairs and undergoes a pair-instability supernova (PISN). In this case the star is completely disrupted and no remnant is left (Fowler & Hoyle 1964). While the conditions that lead to, or prevent, a successful supernova explosion are not yet fully understood (see e.g. O’Connor & Ott 2011; Müller, Janka & Heger 2012), the evolution of *binary* massive stars is even less certain. The binary orbit is thought to decay during a common envelope phase (Podsiadlowski 2001; Ivanova et al. 2013) with a possible contribution from a chemically homogeneous evolution channel (Mandel & de Mink 2016; Marchant et al. 2016). A complementary channel for binary BH formation, driven by mergers in dense stellar environments, may become dominant in stellar clusters (e.g. Ziosi et al. 2014; Antonini & Rasio 2016; Rodriguez, Chatterjee & Rasio 2016; Gerosa & Berti 2017; Fujii, Tanikawa & Makino 2017). Other possible scenarios for forming stellar-mass binary BHs include primor-

* E-mail: dvorkin@iap.fr

dial BHs (Bird et al. 2016; Sasaki et al. 2016) and population III remnants (Kinugawa et al. 2014; Hartwig et al. 2016; Inayoshi et al. 2016). The distributions of masses, spins and redshifts of detectable sources in each of these channels are different, which opens the possibility of studying them with upcoming GW observations. However, the number densities of sources also depend on the underlying galaxy evolution model, for example the star formation rate (SFR), as well as other (sometimes ill-constrained) parameters, which renders model selection rather challenging.

Nevertheless, several groups have recently started to explore the full potential of GW observations for stellar evolution modeling, in particular for constraining the parameters of specific models (e.g. Belczynski et al. 2016a; Wysocki et al. 2017) as well as model selection (Zevin et al. 2017; Gerosa & Berti 2017; Hotokezaka & Piran 2017) and direct probing of the BH mass function (Kovetz et al. 2017). Notably, the important issue of the properties of galaxies that host binary BH mergers has been discussed by Lambergs et al. (2016) and Schneider et al. (2017).

In this article we propose a general framework for the analysis of future GW observations. Our ultimate goal is to be able to constrain a large variety of stellar evolution scenarios which will be embedded in our galaxy evolution model. For the latter we use the model developed in Dvorkin et al. (2016b) and Dvorkin et al. (2016a) (based on Daigne et al. 2004, 2006; Vangioni et al. 2015) and implement several stellar evolution models that we wish to compare. We then estimate the number of detections that would be made by LIGO in each case, as well as the mass and redshift distribution of these *detectable* mergers.

Our semi-analytic approach is unique in that it will allow us to marginalize over many astrophysical 'nuisance parameters', such as the star formation rate (in particular at high redshifts, where it is poorly constrained), the binary fraction of black holes, their time to coalescence etc. This article describes our astrophysical framework and makes a qualitative comparison between several stellar evolution models. We leave a more quantitative statistical analysis to future work, which will also include a forecast on the number of detections needed to exclude these stellar evolution models.

The structure of this paper is as follows. Section 2 describes our calculation of detection rates of binary BH mergers. Section 3 details our galaxy evolution model as well as the four stellar evolution models which we implement here. Our results for the mass and redshift distribution of *detectable* mergers are presented in Section 4. Finally, we discuss future applications of our framework in Section 5.

2 DETECTION RATES

We start with a model (to be specified below) that provides the total birth rate of BHs per unit *observer* time per unit comoving volume V and per unit BH mass m :

$$\frac{dn_{tot}}{dm} = \frac{dN}{dt_{obs} dV dm}. \quad (1)$$

We then assume that only a fraction $\beta(m)$ of these BHs reside in binary systems that coalesce within a Hubble time:

$$\frac{d\dot{n}_2}{dm}(m) = \beta(m) \frac{dn_{tot}}{dm}. \quad (2)$$

Then the birth rate of binaries with component masses m and $m' \leq m$ reads:

$$\frac{d^2\dot{n}_{bin}}{dm dm'}(m, m') = \frac{d\dot{n}_2}{dm} \frac{d\dot{n}_2}{dm'} P(m', m) \quad (3)$$

where δ is the Dirac distribution. The function $P(m', m)$ is normalized so that:

$$\int \frac{d\dot{n}_2}{dm} \frac{d\dot{n}_2}{dm'} P(m', m) dm' dm = \frac{1}{2} \int \frac{d\dot{n}_2}{dm} dm. \quad (4)$$

If the binary merges within a time t_{delay} after it has formed, where the latter is given by the normalized probability distribution $P_d(t_{delay})$:

$$\int_{t_{min}}^{t_{max}} P_d(t_{delay}) dt_{delay} = 1, \quad (5)$$

then the number of binaries merging per unit time $t_{merge} = t + t_{delay}$ is given by:

$$\frac{dN}{dt_{merge} dm dm'} = \int \frac{d^2\dot{n}_{bin}(t)}{dm dm'} P_d(t_{merge} - t) \frac{dV}{dz} dz dt_{obs}. \quad (6)$$

In the last expression, the birth time t and the corresponding redshift z are related by

$$\left| \frac{dt}{dz} \right| = \frac{1}{H_0 \sqrt{\Omega_m(1+z)^3 + \Omega_\Lambda(1+z)}} \quad (7)$$

and t_{obs} is the observation time. Since the total observation time is very short compared to cosmological scales ($T_{obs} \sim 50$ days for LIGO O1+O2), the integral over dt_{obs} is trivial. In order to obtain the number of events detectable by a given instrument, e.g. Advanced LIGO, we need to calculate the signal-to-noise rate (SNR) for each of these events:

$$\rho^2 = 4 \int \frac{|h(f)|^2}{S_n(f)} df \quad (8)$$

where $h(f)$ is the GW strain in the observed frequency domain and $S_n(f)$ is the noise power spectral density. Note that the strain is a function of the binary parameters: component masses and spins, redshift, orientation and sky localization. We obtain the number of observed events (defined here as those with $\rho > 8$) by first calculating $P(\rho > 8|m_1, m_2, z)$, the probability that a merger of BHs with masses m_1 and m_2 at redshift z is detectable. We average over source orientation and component spins (assuming they are distributed isotropically). It follows that the number of sources detectable after observing for a total time T_{obs} is:

$$\frac{dN_{det}}{dt_{merge} dm dm'} = T_{obs} \int \frac{d^2\dot{n}_{bin}}{dm dm'} P_d(t_{merge} - t) P(\rho > 8|m, m', z_{merge}) \frac{dV}{dz} dz \quad (9)$$

In this work we assume the following distributions:

$$P(m', m) = \text{constant}, \quad m, m' \in [M_{min}, M_{max}] \quad (10)$$

and

$$P_d(t_{delay}) \propto \frac{1}{t_{delay}}, \quad t \in [t_{min}, t_{max}] \quad (11)$$

with $t_{min} = 50$ Myr and $t_{max} = t_H$, where t_H is the Hubble time. Furthermore we assume that the fraction of BHs that are in binaries and that merge within a Hubble time is $\beta = 0.01$ and does not depend on mass.

In order to calculate the SNR from eq. (8) we use the *PhenomB* inspiral-merger-ringdown waveforms (Ajith et al. 2011) and the noise power spectral density from Abbott et al. (2016c). Finally, we assume that the instrument sensitivity was constant across O1 and O2.

In order to compare our model predictions to observational data we present below the detection rate in the primary mass-secondary mass plane:

$$R_{\text{det}}(m, m') = \frac{1}{T_{\text{obs}}} \int \frac{dN_{\text{det}}}{dt_{\text{merge}} dm dm'} dt_{\text{merge}}. \quad (12)$$

In the next Section we discuss the astrophysical models that provide the birth rate of binary BHs.

3 ASTROPHYSICAL MODELS

3.1 Galaxy evolution

There are two astrophysical terms in eq. (9): the birth rate of binaries $d\dot{n}/dmdm'$ and the probability to merge after a time delay t_{delay} given by $P(t_{\text{delay}})$. Some of the current stellar evolution models can predict the birth rate of binaries with a certain set of orbital parameters, from which the merging time due to emission of GW can be calculated (Belczynski et al. 2010, 2016b). Other models provide only the birth rate $d\dot{n}/dmdm'$ and have to rely on some distribution of merging times $P(t_{\text{merge}})$. Moreover, most astrophysical models utilize some distribution of the component masses of the stellar binary as an input. It should also be kept in mind that the birth rate of BHs follows from the formation rate of their progenitor massive stars and so depends on the global star formation rate and the stellar initial mass function, as well as stellar metallicity and local density (for example, multiple mergers can occur in dense stellar environments). Therefore, the stellar evolution model that we wish to test needs to be embedded in a galaxy evolution framework, either (semi-)analytical or numerical.

In this work we rely on the semi-analytic approach developed in Dvorkin et al. (2016b) and Dvorkin et al. (2016a), which is based on the galaxy evolution model in Daigne et al. (2004, 2006) and Vangioni et al. (2015). To sum up, our model takes as an input the structure formation history (computed with the Press-Schechter semi-analytic approach), the star formation rate (SFR) history, the initial mass function and stellar yields. Another crucial input is the relation between initial stellar mass and metallicity and the remnant (neutron star or black hole) mass. The latter component is taken from detailed stellar evolution models that we want to test, as described below. The output of our model is the evolution of the chemical composition of the interstellar and circumgalactic media and the number densities of black holes and neutron stars, as well as other astrophysical quantities, i.e. gas fraction and the optical depth to reionization, used to calibrate the model. We assume the Salpeter stellar initial mass function (Salpeter 1955) in the mass range $0.1 - 100 M_{\odot}$ and calibrate our SFR to the observations compiled by Behroozi, Wechsler & Conroy (2013), complemented by those by Bouwens et al. (2015) and Oesch et al. (2015), as described in Vangioni et al. (2015). We use the metal yields from Woosley & Weaver (1995) for all of our models. Further discussion on the constraints on metallicity

evolution and SFR, as well as a more detailed model description, can be found in Dvorkin et al. (2016b).

3.2 Stellar evolution and initial mass-remnant mass relation

In order to relate the initial stellar mass to the remnant mass we used four stellar evolution models: (1) the *Fryer* model, based on the *delayed* model in Fryer et al. (2012); (2) the *WWp* model, based on Woosley & Weaver (1995); and (3)-(4), two models from Limongi (2017) with and without stellar rotation, which we name *Limongi300* and *Limongi*, respectively. All of these models provide the remnant mass as a function of initial stellar mass and metallicity. Since we use Woosley & Weaver (1995) to calculate stellar yields in all of these cases, the *WWp* model is the most consistent choice. Note, however, that it is based on rather old 'piston' pre-collapse stellar models and assumes a constant explosion energy. Recent studies suggested that the explosion is powered by neutrinos stored behind the shock (Fryer & Kalogera 2001; Fryer et al. 2012). In this picture the explosion energy depends on neutrino heat transport mechanisms, the nature of the hydrodynamic instabilities that convert neutrino thermal energy to kinetic energy that can power the supernova (e.g. Blondin, Mezzacappa & DeMarino 2003), and the resulting time delay between shock bounce and explosion. Fryer et al. (2012) provide an analytic model for the latter and calculate the explosion energy, as well as the remnant mass, using numerical pre-collapse stellar models from Woosley, Heger & Weaver (2002). Here we use the *delayed* model from Fryer et al. (2012) as a representative case.

Limongi (2017) presents a different set of models, including the cases of rotating stars. These models differ from the ones in Fryer et al. (2012) in two aspects. First, Limongi (2017) uses a different set of pre-collapse stellar models which vary from Woosley, Heger & Weaver (2002) in their treatment of convection, mass-loss rate and angular momentum transport. For example, the metallicity dependence of the mass-loss rate used in Fryer et al. (2012) is $\dot{M} \propto Z^{0.5}$, where Z is the metallicity (Kudritzki et al. 1989), whereas Limongi (2017) use the steeper relation obtained in Vink, de Koter & Lamers (2001): $\dot{M} \propto Z^{0.85}$. Second, Limongi (2017) assumed a constant explosion energy in the calculation of the remnant mass, similar to the approach of Woosley & Weaver (1995) and contrary to Fryer et al. (2012). As we will see below, these differences amount to significant discrepancies in the mass distribution of *detectable* BHs among the *Fryer* and *Limongi* models.

Finally, the *Limongi300* model allows us to test the effect of rotation of the distribution of remnant masses. Rotation affects the evolutionary path of a massive star by lowering the effective gravity and inducing rotation-driven mixing. According to the results of Limongi (2017), the main effect of rotation on the resulting BH mass is to reduce the minimal mass required for the PISN stage therefore limiting the maximal BH mass. In order to test this model we assumed that all the stars rotate at 300 km/sec (rather than using a distribution of velocities).

The initial mass-remnant mass relation for these models is shown in Figure 1. There is a clear 'mass hierarchy' among the models, with the exception of *Limongi300* which exhibits a cutoff at $M_{\text{star}} \sim 70 M_{\odot}$. This is the result of the

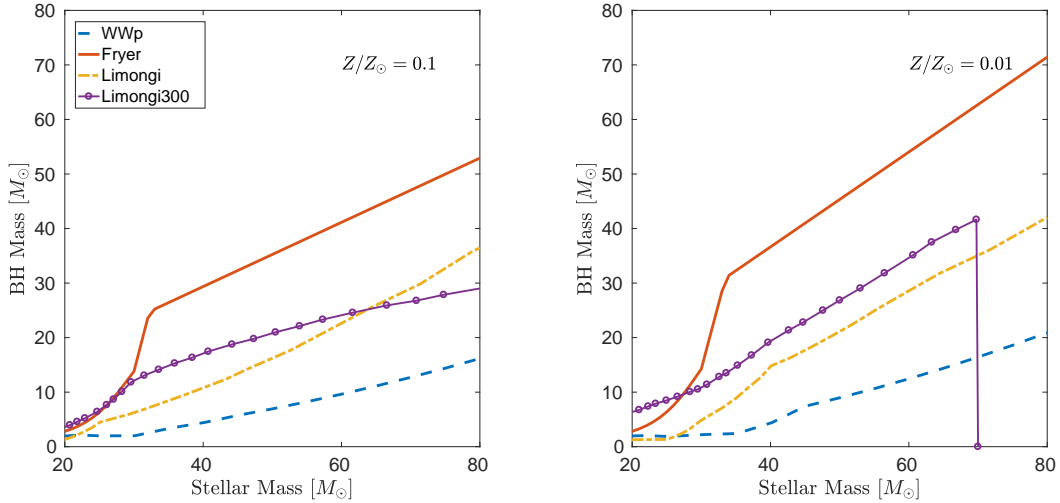


Figure 1. Initial mass-remnant mass relation for the stellar models used in this work for two metallicity values, $Z = 0.1Z_{\odot}$ (left panel) and $Z = 0.01Z_{\odot}$ (right panel). Note that the BH masses are higher in the lower-metallicity case, except for the *Limongi300* model which exhibits a cutoff at $M \sim 70M_{\odot}$ (see text for discussion).

fact that rotating stars enter the pair-instability regime at lower masses than non-rotating stars, as can be seen in Figs. 24g and 24i in [Limongi \(2017\)](#). Note also the nearly vertical relationship obtained in the *Fryer* model around $M_{\text{star}} \sim 30$. This is the result of the prescription for stellar winds adopted in this model (see their Eq. (7) and Fig. 4). We will see below that this feature creates an imprint on the observed BH mass distribution. Note also that in all the cases the BH masses are higher at low metallicity, as expected in view of the reduced stellar winds.

3.3 Merger rate calculation

In order to evaluate the total number of observed events from Eq. (9) we construct lightcones up to $z = 15$ and calculate the mean expected number of events $\langle N_{\text{bin}} \rangle(t_{\text{merge}}, m, m')$ in bins of primary and secondary masses m, m' , volume shells $\frac{dV}{dz} \frac{dz}{dt} \Delta t$ (where $\Delta t = 250$ Myr) and merging times $\Delta t_{\text{merge}} = 250$ Myr. Finally, we sum over all birth times t_{birth} to obtain the distribution of sources in the mass-redshift space.

We can also calculate the *observed* merger rate density from the number of actual LIGO detections and assuming a specific astrophysical model. For this purpose we use the procedure outlined in [Abbott et al. \(2016a\)](#) (see their Appendix C). Namely, if Λ is the number of LIGO triggers of astrophysical origin, then it is related to the merger rate density through:

$$\Lambda_1 = R \langle VT_{\text{obs}} \rangle \quad (13)$$

where $\langle VT_{\text{obs}} \rangle$ is the population-averaged sensitive space-time volume of search (Eq. C3 in [Abbott et al. \(2016a\)](#)):

$$\langle VT_{\text{obs}} \rangle = T_{\text{obs}} \int dz d\theta \frac{dV_c}{dz} \frac{1}{1+z} s(\theta) f(z, \theta), \quad (14)$$

$s(\theta)$ is the normalized distribution function of the BH population with respect to the parameters θ (for example mass)

and $f(z, \theta)$ is a selection function that gives the probability of detecting a source with parameters θ at redshift z . We stress that since $s(\theta)$ is a normalized distribution, our choice of β , the fraction of BHs that are in binaries and that merge within a Hubble time (see Eq. (2)) does not influence our results.

Note that the deduced merger rate density depends on the astrophysical model assumed for the analysis. For example, if we used an astrophysical model that predicts a negligible *relative* number of $\sim 30M_{\odot}$ BHs, LIGO detections would imply a *high* total merger rate to allow for the detected $\sim 30M_{\odot}$ events. Conversely, assuming a model that produces an over-abundance of $\sim 30M_{\odot}$ BHs would result in a *low* overall merger rate.

4 RESULTS

The simplest way to compare between the four stellar evolution models discussed above is to calculate the detection rate of binary BH mergers that implied from the detections made during the Advanced LIGO O1+O2 observing runs, as outlined in Section 3.3. As can be seen in Table 1, these range from 15 to 59 $\text{Gpc}^{-3} \text{yr}^{-1}$ and are in all the cases smaller than the one obtained in [Abbott et al. \(2016a\)](#) ($97^{+135}_{-67} \text{ Gpc}^{-3} \text{yr}^{-1}$ for their power-law model). Several factors could contribute to this discrepancy. First, [Abbott et al. \(2016a\)](#) assume that the sources are distributed uniformly in comoving volume, whereas our model predicts a specific redshift evolution that peaks at $z \sim 2$ ([Dvorkin et al. 2016b](#)). Therefore our model predicts lower relative numbers of low-redshift sources. Second, the BH mass function in our models differs from the one in ([Abbott et al. 2016a](#)) because here we examine various initial mass-remnant mass relations, as discussed above. Finally, we note that our treatment of the selection function $f(\theta)$ is oversimplified with respect to the analysis of [Abbott et al. \(2016a\)](#). In view of the uncertainty in the astrophysical model, it is also unclear which of these

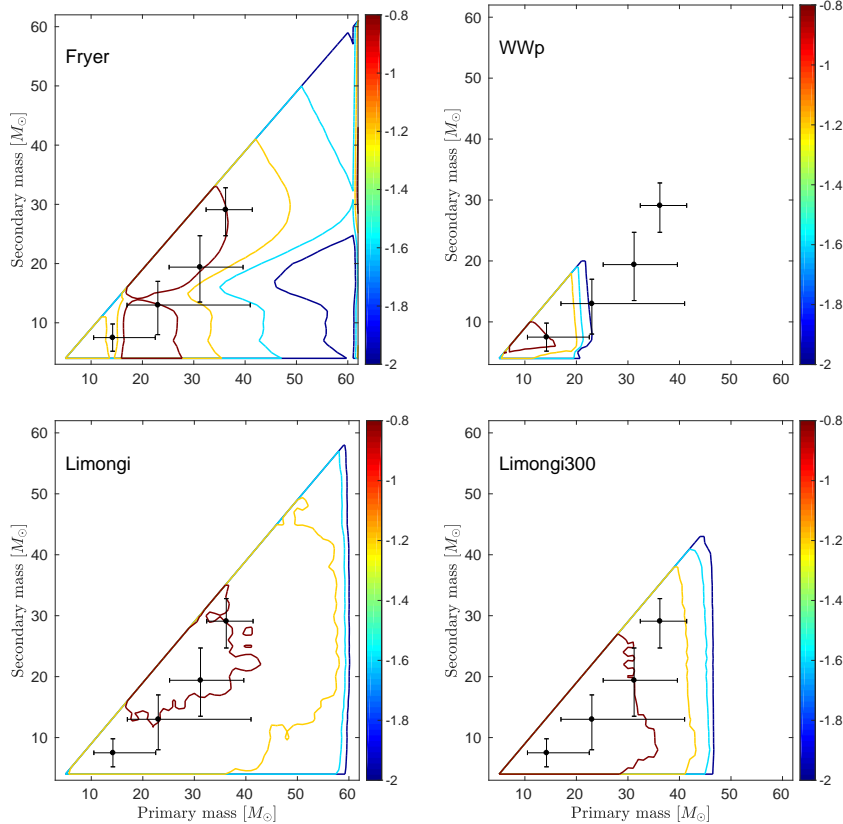


Figure 2. Mass distribution of merging binary BHs in the astrophysical models considered in this paper: *Fryer* (upper left), *WWp* (upper right), *Limongi* for non-rotating stars (lower left) and *Limongi* with all stars rotating at 300 km/s (lower right). Color coded is $\log_{10} R_{\text{det}}$ where R_{det} is the detection rate in units of $[M_{\odot}^{-2} \text{yr}^{-1}]$ (see Eq. (12)). The data points correspond to the published LIGO detections (including one event slightly below the discovery threshold). All the masses are in the source frame.

Table 1. Merger rates deduced from LIGO observations assuming different astrophysical models (see text for discussion).

	Rate $[Gpc^{-3} \text{yr}^{-1}]$
Fryer	18
WWp	59
Limongi	15
Limongi300	32

interpretations is correct, but it is important to keep in mind that the merger rates computed from the observed number of events are model-dependent. These results may be important for predicting the level of the expected stochastic background of GW (Abbott et al. 2016b), although we note that the observational uncertainties, due to the small number of events, are still more significant than the modeling uncertainty.

In Figure 2 we plot the contours of constant detection rates per unit mass squared (in units of events per yr per M_{\odot}^2) for each of our models in the $M_1 - M_2$ plane, where M_1 and M_2 are the primary and secondary BH masses, respectively (see Eq. (12)). We also show the events detected by LIGO by black points with error bars. For example, comparing the first LIGO detection GW150914 with our models, we see that the *Fryer* model predicts ~ 0.16 such detections per year per M_{\odot}^2 which, taking into account the error bars on the

observed masses and the O1 coincident analysis time of 51.5 days, gives ~ 1 expected detections in this model. The same calculation applies to the *Limongi* models, but the *WWp* case clearly produces too few BHs above $\sim 25M_{\odot}$. It is important to mention that these results depend on our model parameter β (the number of BHs that are in binaries and that merge within a Hubble time). However we stress that the relative mass distribution is not affected by our choice of β as long as it is taken to be a constant. Our value $\beta = 0.01$ was chosen to roughly correspond to most of the models considered here. The only exception is *WWp* which cannot be accommodated even with the maximal (and unrealistic) value of $\beta = 1$.

However, the most interesting (and robust) conclusion from our calculation is that the models discussed here present various specific features in their mass distributions of detectable BHs. For example, the *WWp* and the *Limongi300* models produce negligible number densities of BHs with masses above $\sim 25M_{\odot}$ and $\sim 45M_{\odot}$, respectively. This means that these models can be excluded even with a very small number of detections of 'heavy' sources.

The case of the *Fryer* and *Limongi* models is even more striking: while they produce nearly identical *total* numbers of detectable mergers, the mass distribution of these events is quite different. Specifically, in the *Fryer* model the detectable binaries tend to cluster around $\sim 20 - 30M_{\odot}$. This feature of the *Fryer* model can be traced back to the

fact that in this description more massive stars experience stronger winds in such a fashion as to create an accumulation of BH masses at $\sim 20 - 30M_{\odot}$, as can be seen from Fig. 4 and eq. (7) in Fryer et al. (2012) and Figure 1 above. On the other hand, the mass distribution of *detectable* sources in the *Limongi* model is predicted to be almost flat, with the exception of a small 'island' at $M \sim 20 - 40M_{\odot}$, possibly because in this model the reduced number densities of more massive BHs are roughly compensated by the fact that they are easier to detect. In this case, a large number of detections of $\sim 10M_{\odot}$ sources will probably exclude the *Fryer* model while favouring the *Limongi* model.

With only $3 + 1$ detected events, we clearly cannot rule out any of these models, but it may be possible when the number of detections will increase. We can then study their mass distribution looking for specific features: do the sources cluster around specific mass values? Is there a mass cutoff? In particular, it might be interesting to estimate the number of detections necessary to rule out specific models, and we plan to do it in an upcoming paper. A possible caveat to this approach is that several channels for BH formation (i.e. primordial BHs, PopIII remnants, dynamical formation) may co-exist, rendering the distribution even more complex.

We note that in our approach, the galaxy evolution processes, including the SFR and the metallicity evolution are the same for all the models, and the differences in the resulting distribution of BH masses can be directly attributed to differences in the stellar evolution model. On the other hand, our framework gives us the ability to marginalize over the unknown astrophysical parameters. As a qualitative example, we show in Figure 3 the effect of varying the distribution of delay times for the *Limongi* model. Specifically, we show three distributions: $1/t_{\text{delay}}$ (left), *const.* (center) and Gaussian with mean 1 Gyr and width 1 Gyr (right). The *const.* distribution is results in a rather different mass distribution than the other two, in particular at lower masses, but it is less likely according to standard models of binary evolution which favor a $1/t_{\text{delay}}$ distribution. A complete rigorous statistical analysis is needed in order to evaluate whether it will be possible to marginalize over the (unknown) time delay distribution, or whether some preliminary assumptions are necessary.

In addition to the distribution of detectable sources in the $M_1 - M_2$ plane we can calculate their redshifts. Fig. 4 shows the contours of constant detection rates in the $M_c - z$ plane, where the chirp mass is $M_c = (M_1 M_2)^{3/5} / (M_1 + M_2)^{1/5}$. Combining these predictions with those from Figure 2 will result in even tighter constraints. As in the case of the $M_1 - M_2$ plane, the *Fryer* and *Limongi* models seems to provide a better correspondence to LIGO detections.

5 DISCUSSION

The discovery of GW from merging binary BHs opens new perspectives for the studies of stellar evolution and BH formation. In this paper we introduced a framework that can be used to analyze upcoming GW detections in a full astrophysical context with the aim of constraining stellar evolution models. We qualitatively showed the effect of different models on the mass and redshift distribution of potential LIGO sources. We find that among the stellar evolution models dis-

cussed here the *Limongi* model without stellar rotation and the *Fryer* model provide the best description of the observed distribution. These models differ in the mass distribution of *detectable* BHs: while the *Fryer* model predicts a concentration of BHs around $\sim 20 - 30M_{\odot}$ (a result of the modeling of mass loss in this case), the distribution is almost flat in the *Limongi* model. It therefore seems possible to discriminate between these models with more observations of BH mergers. We also find that the *WWp* model is not compatible with LIGO detections since it produces too few BHs above $\sim 25M_{\odot}$. Moreover, the *Limongi300* model, in which all the stars rotate at 300 km/sec is also unlikely due to a cutoff it introduces at $\sim 45M_{\odot}$, which is a result of the fact that rotating stars undergo PISN at lower masses than their non-rotating counterparts.

Having made these qualitative statements, we emphasize that a rigorous statistical treatment is necessary in order to fully exploit the potential of this approach, which we plan to provide in future work. It is also interesting to consider alternative BH formation channels, such as the dynamical formation channel, PopIII remnants and primordial BHs. In view of our results, it is clear that models which present specific unique features in their mass and/or redshift distribution will be the easiest to constrain. For example, even a single $\sim 150M_{\odot}$ BH could point to one of these alternative channels, since it cannot be produced via standard stellar evolution (as it would fall in the PISN range). However, in the absence of such 'smoking-gun' detections and in view of the large variety of stellar evolution models it might be difficult to constrain some of these alternative channels with current ground-based interferometers. For example, the primordial BH scenario seems to be difficult to constrain if the merger times are distributed roughly like $1/t_{\text{delay}}$ as in Sasaki et al. (2016) (and similarly to the stellar-origin BHs), and the BH mass function is bottom-heavy with a cutoff at $\sim 70M_{\odot}$ as in Carr, Tenkanen & Vaskonen (2017). While the redshift distribution of these sources will be constant out to high redshifts, contrary to the case of stellar-origin BHs, this feature will not be detectable before the next generation of ground-based interferometers becomes operational (see Appendix A for a example of the mass distribution of detectable primordial BHs).

Finally, we have not discussed the spins of the merging BHs, which can provide additional constraints, in particular for the dynamical formation channel, and which we plan to include in future work.

ACKNOWLEDGMENTS

ID is grateful to Thibaut Louis for useful discussions. This work has been done within the Labex ILP (reference ANR-10-LABX-63), part of the Idex SUPER, and received financial state aid managed by the Agence Nationale de la Recherche, as part of the programme Investissements d'avenir under the reference ANR-11-IDEX-0004-02. We acknowledge the financial support from the EMERGENCE 2016 project, Sorbonne Universités, convention no. SU-16-R-EMR-61 (MODOG).

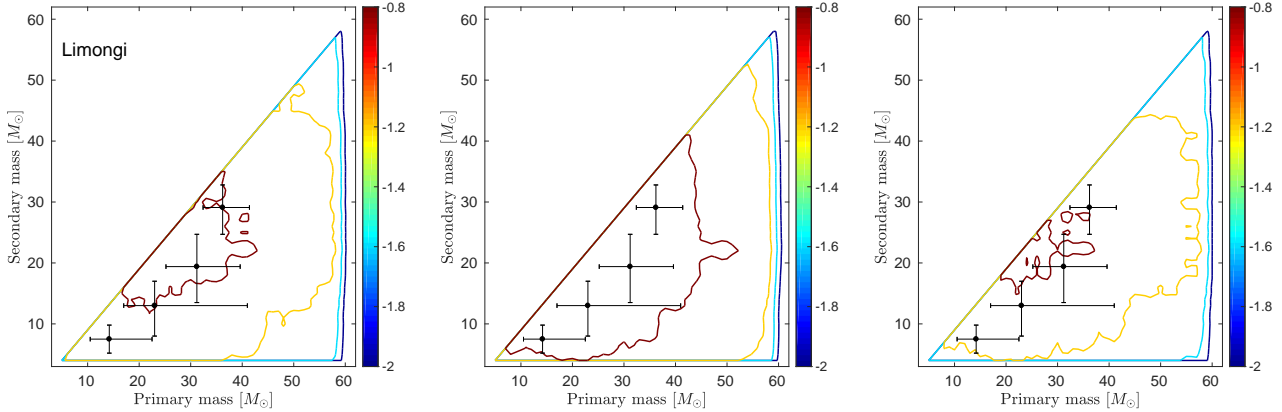


Figure 3. Same as Fig. 2 for the *Limongi* model with different time delay distributions in Eq. (11): $1/t_{\text{delay}}$ (left panel), a constant distribution (middle panel) and a Gaussian distribution with mean 1 Gyr and variance 1 Gyr.

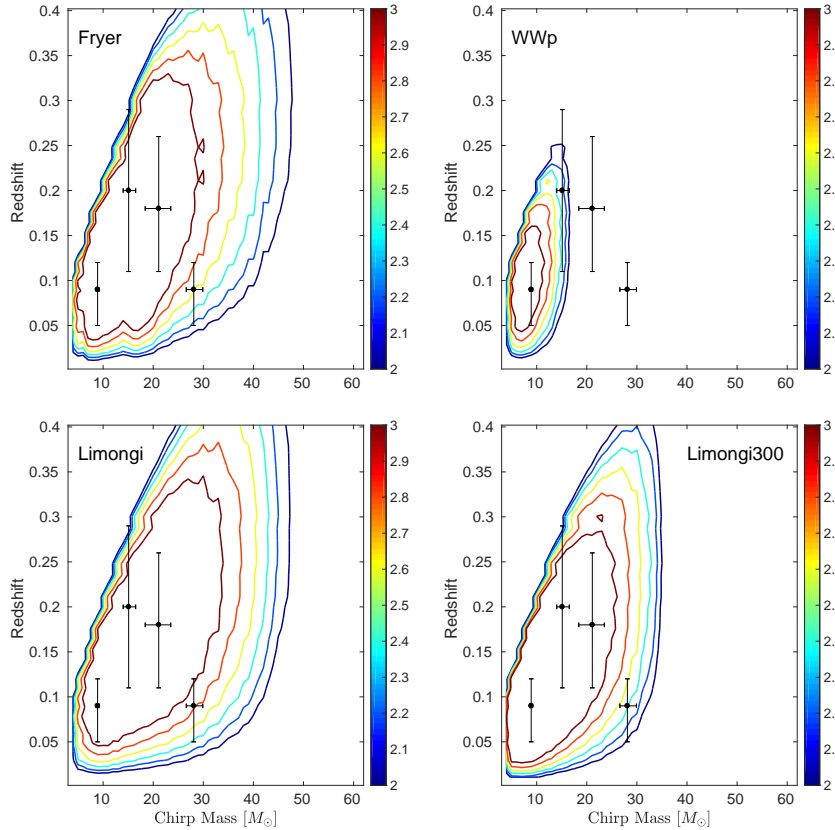


Figure 4. Distribution of detectable events in the merger redshift-chirp mass plane for the astrophysical models considered in this work. Color coded is $\log_{10}(dR_{\text{det}}/dz)$ where dR_{det}/dz is the detection rate in units of $[M_{\odot}^{-1} \text{yr}^{-1}]$. The data points correspond to the published LIGO detections (including one event slightly below the discovery threshold). All the masses are in the source frame.

REFERENCES

Abbott B. P. et al., 2016a, Physical Review X, 6, 041015
 Abbott B. P. et al., 2016b, Physical Review Letters, 116, 131102
 Abbott B. P. et al., 2016c, Physical Review Letters, 116, 131103
 Abbott B. P. et al., 2016d, Physical Review Letters, 116, 061102
 Abbott B. P. et al., 2017, Physical Review Letters, 118, 221101
 Ajith P. et al., 2011, Physical Review Letters, 106, 241101
 Ali-Haïmoud Y., Kamionkowski M., 2017, Phys. Rev. D, 95, 043534
 Ali-Haïmoud Y., Kovetz E. D., Kamionkowski M., 2017, ArXiv e-prints
 Antonini F., Rasio F. A., 2016, ApJ, 831, 187
 Behroozi P. S., Wechsler R. H., Conroy C., 2013, ApJ, 770, 57
 Belczynski K., Dominik M., Bulik T., O'Shaughnessy R.,

Fryer C., Holz D. E., 2010, *ApJ*, 715, L138

Belczynski K. et al., 2016a, *A&A*, 594, A97

Belczynski K., Holz D. E., Bulik T., O'Shaughnessy R., 2016b, *Nature*, 534, 512

Bird S., Cholis I., Muñoz J. B., Ali-Haïmoud Y., Kamionkowski M., Kovetz E. D., Raccanelli A., Riess A. G., 2016, *Physical Review Letters*, 116, 201301

Blondin J. M., Mezzacappa A., DeMarino C., 2003, *ApJ*, 584, 971

Bouwens R. J. et al., 2015, *ApJ*, 803, 34

Carr B., Tenkanen T., Vaskonen V., 2017, ArXiv e-prints

Carr B. J., Gilbert J. H., Lidsey J. E., 1994, *Phys. Rev. D*, 50, 4853

Daigne F., Olive K. A., Silk J., Stoehr F., Vangioni E., 2006, *ApJ*, 647, 773

Daigne F., Olive K. A., Vangioni-Flam E., Silk J., Audouze J., 2004, *ApJ*, 617, 693

Dvorkin I., Uzan J.-P., Vangioni E., Silk J., 2016a, *Phys. Rev. D*, 94, 103011

Dvorkin I., Vangioni E., Silk J., Uzan J.-P., Olive K. A., 2016b, *MNRAS*, 461, 3877

Fowler W. A., Hoyle F., 1964, *ApJS*, 9, 201

Fryer C. L., Belczynski K., Wiktorowicz G., Dominik M., Kalogera V., Holz D. E., 2012, *ApJ*, 749, 91

Fryer C. L., Kalogera V., 2001, *ApJ*, 554, 548

Fujii M., Tanikawa A., Makino J., 2017, ArXiv e-prints

Gerosa D., Berti E., 2017, *Phys. Rev. D*, 95, 124046

Hartwig T., Volonteri M., Bromm V., Klessen R. S., Baurasse E., Magg M., Stacy A., 2016, *MNRAS*, 460, L74

Hotokezaka K., Piran T., 2017, ArXiv e-prints

Inayoshi K., Kashiyama K., Visbal E., Haiman Z., 2016, *MNRAS*, 461, 2722

Ivanova N. et al., 2013, *A&A Rev.*, 21, 59

Kinugawa T., Inayoshi K., Hotokezaka K., Nakauchi D., Nakamura T., 2014, *MNRAS*, 442, 2963

Kovetz E. D., Cholis I., Breysse P. C., Kamionkowski M., 2017, *Phys. Rev. D*, 95, 103010

Kudritzki R. P., Pauldrach A., Puls J., Abbott D. C., 1989, *A&A*, 219, 205

Lamberts A., Garrison-Kimmel S., Clausen D. R., Hopkins P. F., 2016, *MNRAS*, 463, L31

Limongi M., 2017, ArXiv e-prints

Mandel I., de Mink S. E., 2016, *MNRAS*, 458, 2634

Marchant P., Langer N., Podsiadlowski P., Tauris T. M., Moriya T. J., 2016, *A&A*, 588, A50

Müller B., Janka H.-T., Heger A., 2012, *ApJ*, 761, 72

O'Connor E., Ott C. D., 2011, *ApJ*, 730, 70

Oesch P. A., Bouwens R. J., Illingworth G. D., Franx M., Ammons S. M., van Dokkum P. G., Trenti M., Labb   I., 2015, *ApJ*, 808, 104

Podsiadlowski P., 2001, in *Astronomical Society of the Pacific Conference Series*, Vol. 229, *Evolution of Binary and Multiple Star Systems*, Podsiadlowski P., Rappaport S., King A. R., D'Antona F., Burderi L., eds., p. 239

Rodriguez C. L., Chatterjee S., Rasio F. A., 2016, *Phys. Rev. D*, 93, 084029

Salpeter E. E., 1955, *ApJ*, 121, 161

Sasaki M., Suyama T., Tanaka T., Yokoyama S., 2016, *Physical Review Letters*, 117, 061101

Schneider R., Graziani L., Marassi S., Spera M., Mapelli M., Alparone M., de Bennassuti M., 2017, ArXiv e-prints

Vangioni E., Olive K. A., Prestegard T., Silk J., Petitjean P., Mandic V., 2015, *MNRAS*, 447, 2575

Vink J. S., de Koter A., Lamers H. J. G. L. M., 2001, *A&A*, 369, 574

Woosley S. E., Heger A., Weaver T. A., 2002, *Reviews of Modern Physics*, 74, 1015

Woosley S. E., Weaver T. A., 1995, *ApJS*, 101, 181

Wysocki D., Gerosa D., O'Shaughnessy R., Belczynski K., Gladysz W., Berti E., Kesden M., Holz D., 2017, ArXiv e-prints

Zevin M., Pankow C., Rodriguez C. L., Sampson L., Chase E., Kalogera V., Rasio F. A., 2017, ArXiv e-prints

Ziosi B. M., Mapelli M., Branchesi M., Tormen G., 2014, *MNRAS*, 441, 3703

APPENDIX A: DETECTION RATES OF PRIMORDIAL BLACK HOLES

In this Appendix we modify our formalism to accommodate the case of primordial BHs (PBHs). This scenario is different from all the standard formation channels (i.e. stellar-origin BHs, PopIII remnants and dynamical formation) in that PBHs form at very early times (at around the matter-radiation equality epoch or earlier, e.g. [Carr, Gilbert & Lidsey 1994](#)). There is currently no consensus in the literature regarding the exact mechanism by which PBHs can form, their number density, binary fraction and mass distribution. Nevertheless, they still represent a viable alternative to the standard formation scenario and it is interesting to briefly review the detection rates expected from this population.

Let us assume that all PBHs were formed at the epoch of matter-radiation equality z_{eq} with a power-law mass function:

$$\frac{dn}{dm} \propto m^{-\alpha} \quad (\text{A1})$$

normalized so that they account for a fraction q of the total dark matter density:

$$\rho_{DM} = \frac{1}{q} \int_{M_{\min}}^{M_{\max}} \frac{dn}{dm} m dm. \quad (\text{A2})$$

Below we will consider the case with $M_{\min} = 10M_{\odot}$, $M_{\max} = 1000M_{\odot}$, $q = 0.01$ (see [Ali-Ha  moud & Kamionkowski 2017](#); [Ali-Ha  moud, Kovetz & Kamionkowski 2017](#), for the mass ranges of PBH that fit current observational constraints) and $\alpha = 2$. We stress that there is a very significant theoretical uncertainty regarding these parameters, and the values we chose here serve an illustrative purpose.

We then assume that a fraction Γ of these PBHs forms binaries per unit observer time:

$$\frac{dn_2}{dm dt_{\text{obs}}} (m, t) = \Gamma(t) \frac{dn}{dm} (m). \quad (\text{A3})$$

We take the comoving number density of PBHs to be constant in time, by implicitly assuming that their merger rate is sufficiently small. Then the *comoving* formation rate of binary PBHs is given by Eq. (3), where we assume $P(m', m) = \text{const.}$ for $m, m' \in [M_{\min}, M_{\max}]$.

To obtain the number density of *mergers* we assume the following probability to merge with a delay t_{delay} (inspired

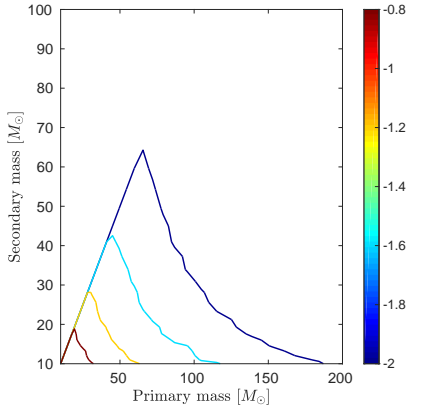


Figure A1. Mass distribution of merging binary PBHs using the phenomenological model discussed in the text, namely 10% of dark matter in PBHs, $P(t) \propto 1/t$ merging time delay distribution, efficiency of binary formation of 10^{-5} per Gyr for $z < 2$ and a power-law mass function with slope $\alpha = 2$ in the mass range $(10-1000)M_\odot$. Color coded is $\log_{10} R_{\text{det}}$ where R_{det} is the detection rate in units of $[M_\odot^{-2} \text{yr}^{-1}]$.

by [Sasaki et al. 2016](#), although note that in their case all the binaries form immediately after the formation of the BHs themselves):

$$P_{\text{d}} \propto \frac{1}{t_{\text{delay}}}. \quad (\text{A4})$$

Then the merger rate per unit time is given by Eq. (6) whereas the number of detectable sources can be calculated using Eq. (9).

Note that we still need to specify Γ , the binary formation rate. For example, the mechanism proposed by [Sasaki et al. \(2016\)](#) corresponds to $\Gamma = \delta(z_{\text{eq}})$ where δ is the delta function, whereas in the scenario of [Bird et al. \(2016\)](#) binary formation occurs predominantly at lower redshift, after halo collapse.

In order to illustrate this formalism we adopt $\Gamma = 10^{-4} \text{ Gyr}^{-1}$ for $z < 2$. This value was chosen so as not to overproduce low-mass BHs (which would be in conflict with LIGO observations), and is therefore an upper limit. The detection rates that would be obtained by LIGO in this case are shown in Figure A1. Due to the bottom-heavy mass function that we selected here, the mass distribution of *detectable* events is also skewed towards lower masses, but the detection rate of $M \sim 150M_\odot$ is not negligible (assuming of course that the PBH mass function extends to these masses). As shown above, such BHs cannot be produced via the standard stellar evolution scenario as they would fall in the PISN range. It seems tempting therefore to suggest that even a single detection of a $M \sim 150M_\odot$ BH would provide a strong hint towards a primordial origin, although more detailed studies are needed in order to exclude other formation scenarios such as the dynamical formation channel.